The location of the grounding zone of Evans Ice Stream, Antarctica, investigated using SAR interferometry and modelling

Helena J. SYKES, Tavi MURRAY, Adrian LUCKMAN

School of the Environment and Society, Swansea University, Singleton Park, Swansea SA2 8PP, UK
E-mail: 366845@swansea.ac.uk

ABSTRACT. Evans Ice Stream, West Antarctica, has five tributaries and a complex grounding zone. The grounding zone of Evans Ice Stream, between the landward and seaward limits of tidal flexing, was mapped using SAR interferometry. The width of the mapped grounding zone was compared with that derived from an elastic beam model, and the tidal height changes derived from interferometry were compared with the results of a tidal model. Results show that in 1994 and 1996 the Evans grounding zone was located up to 100 km upstream of its location in the BEDMAP dataset. The grounding line of Evans Ice Stream is subjected to 5 m vertical tidal forcing, which would clearly affect ice-stream flow.

INTRODUCTION

Evans Ice Stream is a large ice stream with five tributaries, draining a 104 000 km^2 catchment of the West Antarctic ice sheet (WAIS) (Bamber and others, 2000; Joughin and Bamber, 2005). The WAIS is a marine ice sheet with much of its bed below sea level, containing ~6 m of potential sea-level rise. The grounding zone, which marks the transition between an ice sheet and an ice shelf, is an important control on ice-sheet stability as it determines the ice discharge from the grounded ice sheet (e.g. Weertman, 1974; Schoof, 2007). Longitudinal stress in this area prevents a large increase in velocity when basal drag is reduced to zero as the ice starts to float (Bindschadler, 2006). However, grounding lines are often modelled inadequately, due to both coarse ice-sheet model resolution and the use of approximations in models of marine ice sheets, which leads to ice sheets being modelled separately from ice shelves, with boundary conditions imposed at the grounding line (Vieli and Payne, 2005; Schoof, 2007).

It is now widely recognized that the previously held view of an ice-sheet 'grounding line' is an oversimplification, which has been used to refer to several locations (Fig. 1): the landward limit of tidal flexing of the grounded ice stream, also known as the hinge line (F in figure); the limit of flotation (G), which will migrate with the tide, leading to areas between its furthest landward and seaward locations being intermittently grounded at different points in the tidal cycle; the inflexion point (I) and the seaward limit of tidal flexing, which is also the landward limit of the ice-shelf hydrostatic zone (H) (Smith, 1991; Vaughan, 1994; Fricker and Padman, 2006). The grounding zone, or hinge zone, may be defined as the area between F and H, and may be up to several kilometres wide, depending on ice thickness and bed topography.

Locating the grounding zone correctly is important for the interpretation of velocity data, which contain tidal modulation of the signal downstream of F, where Jenkins and others (2006) also found tidal modulation of vertical strain rates and ice thickness on nearby Rutford Ice Stream. More subdued tidal modulation of velocity may also occur considerable distances upstream of F (Anandakrishnan and others, 2003; Bindschadler and others, 2003; Gudmundsson, 2006). Grounding zone migration is monitored to assess the overall stability of the WAIS, but is reliant on the initial location of the grounding zone being correctly identified, as is the accuracy of models using grounding line location as a boundary condition. However, three previously published locations of the Evans Ice Stream grounding line disagree by as much as 93 km (Fig. 2).

Knowledge of the behaviour of the ice streams draining the WAIS is necessary for an accurate assessment of its present and future mass balance and contribution to sea-level rise. Although Evans Ice Stream has the largest discharge of any ice stream feeding the Filchner–Ronne Ice Shelf (FRIS), estimated at $35.7 \pm 3.6\,\mathrm{Gt\,a^{-1}}$ (Joughin and Bamber, 2005), it is the subject of surprisingly little published work. Field expeditions there are hampered by adverse conditions such as crevasse fields and poor visibility (personal communications from E. King, 2006 and E. Morris, 2007). Valuable insight into its dynamics is therefore provided by modelling and by remote-sensing methods, particularly active microwave systems such as synthetic aperture radar (SAR), which is not affected by the presence of cloud and can image through the polar night.

METHODS

Synthetic aperture radar interferometry

SAR interferometry uses the phase difference between successive active microwave satellite scenes to show displacement in the line-of-sight (LOS) direction of the satellite (including both horizontal and vertical displacement)

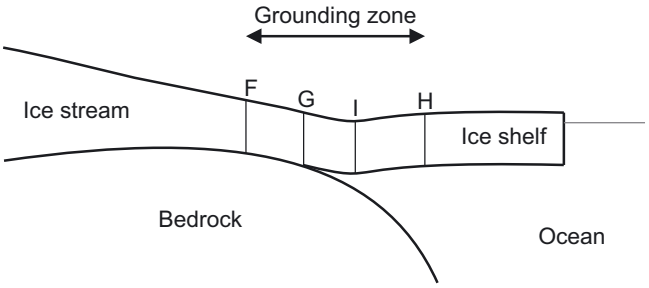

Fig. 1. An ice-shelf grounding zone. F and H mark the landward and seaward limits of tidal flexure, G the limit of flotation and I the inflexion point (after Smith, 1991; Vaughan, 1994; Fricker and Padman, 2006).

https://doi.org/10.3189/172756409789624292 Published online by Cambridge University Press

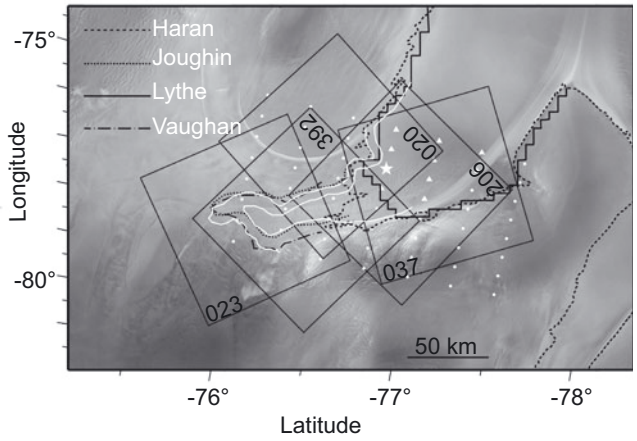

Fig. 2. Previous versions of the grounding line of Evans Ice Stream reported by T. Haran and others (http://nsidc.org/data/nsidc-0280.html), Joughin and others (2006), Lythe and others (2001) and Vaughan and others (2003). The grounding zone mapped in the present study is marked in white. SAR frames are shown and marked with track numbers (Table 1). The white star is the location where tidal components were extracted from the CATS02.01 model. White triangles represent where the CATS02.01 model would run, and white circles indicate locations where it would not, due to its bathymetry grid. The projection is polar stereographic.

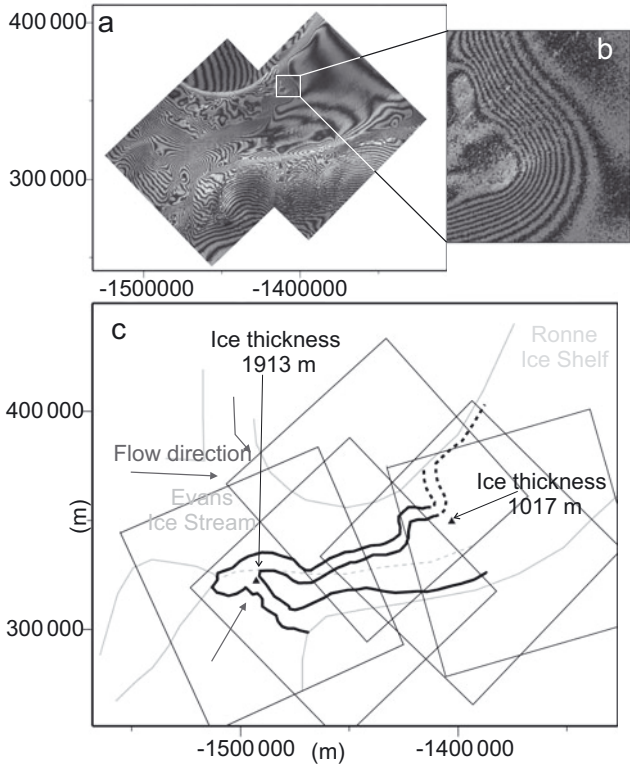

Fig. 3. Grounding zone width of Evans Ice Stream mapped from interferograms. (a) Mosaicked interferograms of tracks 206 and 392. (b) Zoom of the grounding zone in the track 206 interferogram. (c) The grounding zone as mapped from SAR interferometry. Dotted curves indicate mapping from track 206, which also fitted interferograms from tracks 020 and 037; solid curves indicate mapping from a double-difference interferogram of track 392 further upstream. The locations of ice thicknesses used in the elastic beam model are marked as black triangles. SAR frames are shown in black. The dashed grey curve indicates a major flowline. Coordinates are polar stereographic.

and topography. Scenes from the European Remote-sensing Satellites, ERS-1 and ERS-2, were selected for the 'second ice phase' in 1994, and the 'second multidisciplinary phase' in 1996 (Table 1), both of which had short enough orbital repeat periods to maintain coherence, or correlation, between successive scenes, which is a requirement for interferometry.

The phase difference between co-registered scenes of the same frame is calculated for each pixel by multiplying the complex pixel value of one image by the complex conjugate of the other. Phase differences are scaled from 0 to 2π radians. Complete phase cycles are displayed in cycles of colour known as fringes, which are the result of scene topography, LOS displacement and the perpendicular baseline, which is the separation between paired images in the across-track direction. The topographic elevation represented by one fringe is known as the altitude of ambiguity, and for the ERS satellites is calculated by dividing 9416 by the perpendicular baseline (Table 1; NPA Group, http://www.npagroup.com/insar/whatisinsar/insar_simple.htm).

Interferometry, like most methods used to map the grounding zone, identifies F and H (Fig. 1). The high phase gradient in the grounding zone, which occurs because of the change in vertical motion where the ice adjusts to hydrostatic equilibrium at H, means the grounding zone is easily identifiable by its many closely spaced fringes (Rignot, 1998). We digitized the shape and width of the grounding zone in ArcMap from georeferenced interferograms created by the Gamma tools (Fig. 3). Both single- and double-difference interferograms were used; the double-difference interferograms (Zebker and others, 1994), which have had the effects of motion common to two single-difference interferograms removed, proved particularly effective in mapping the grounding zone as they show only differential tidal displacement and scene topography.

The ERS satellites are 2.4 times more sensitive to vertical displacement than horizontal displacement due to their steep look angle, 23°, and each fringe represents ~2.6 cm of vertical displacement if it is assumed all displacement was vertical. Fringes in the grounding zone were counted and the total vertical displacement compared to the tidal change between scenes as predicted by the model (Table 1).

Tidal model

At any given location, the tidal signal can be described as the sum of a number of sine functions representing different diurnal, semi-diurnal and longer-term components, each of which is caused by the gravitational forces between the Sun, the Moon and the Earth. The components of the tidal signal are described according to Doodson numbers, which are integers representing six astronomical phenomena: the Earth's rotation; the Earth's orbit; the Moon's orbit; the periodicity of lunar perigee; lunar orbital tilt; and the location of perihelion in the Earth's orbit (Pawlowicz and others, 2002). These numbers predict the phase and amplitude of the tidal signal were the Earth's response fast enough for the ocean to be in equilibrium with its forcing. Table 2 shows the frequencies of the ten principal tidal components.

The ten principal tidal components for the Evans Ice Stream grounding zone were extracted from the CATS02.01 Circum-Antarctic Tidal Simulation model (Padman and others, 2002) and used with the t_tide model (Pawlowicz and others, 2002) to reconstruct the tidal signal through the time periods

https://doi.org/10.3189/172756409789624292 Published online by Cambridge University Press

Table 1. Tidal height change from the CATS02.01 and t_tide models and as shown by interferograms, for ERS SAR scenes used to map the grounding zone of Evans Ice Stream

Track	Frame	Dates	Perpendicular baseline	Altitude of ambiguity	Tidal height change	Grounding zone fringes	Grounding zone fringes × 2.6
			m	m	cm		cm
020	5553	25–28 Jan. 1994	–102.8	91.60	87	27	70.2
037	5265	23–26 Jan. 1994	–51.6	182.48	–48	10	26.0
206	5535	29–30 Jan. 1996	–143.1	65.80	–38	12	31.2
392	5553	11–12 Feb. 1996	–138.5	67.99	–37	8	20.8

covered by the SAR images (Table 3). The tidal heights at the time of acquisition of each image were used to calculate the difference in tidal height for each interferogram (Table 1).

Elastic beam model

The width of the grounding zone was modelled using an elastic beam model (Vaughan, 1995). The vertical displacement of the ice shelf from its mean position, $w(x)$, was modelled along an x axis perpendicular to and downstream of the grounding line, which, in the model, was clamped in place at $x = 0$. The beam was of uniform thickness. The hinge zone lies between the conditions where w, $\partial w/\partial x$ and $x = 0$ (at the grounding line, in this case meaning F), and $w = A_0(t)$, where $A_0(t)$ is the deviation from mean sea level at a given time, and is given by:

$$w = A_0(t)\left[1 - \mathrm{e}^{-\beta x}\left(\cos\beta x + \sin\beta x\right)\right]. \quad (1)$$

In this equation $A_0(t)$ would be the height of the ice-shelf surface were it floating in hydrostatic equilibrium, and is equivalent to half the tidal range (Smith, 1991). The spatial wavenumber, β, is given by the following equation:

$$\beta^4 = 3\ \rho_{\mathrm{sea}}\ g\ \frac{1 - \nu^2}{Eh^3}, \quad (2)$$

where ρ_{sea} is the sea-water density (taken as $1030\,\mathrm{kg\,m^{-3}}$; Smith, 1991), g is gravitational acceleration, E is the elastic (Young's) modulus, ν is Poisson's ratio and h is the ice-shelf thickness. The spatial wavenumber, β, has a non-linear dependence on h, because changing the ice thickness changes the rigidity of the beam, but β is relatively insensitive to changes in E and ν (Vaughan, 1995; Reeh and others, 2003).

Three different values of E were used: 1.1 GPa, as used by Smith (1991); 0.88 GPa, derived empirically by Vaughan (1995) from analysis of tiltmeter data for several sites in Antarctica; and 9 GPa, as used by Stephenson (1984), which is close to laboratory-derived values of E for ice of 9.3 GPa (Reeh and others, 2003). However, ice thickness about half the real value had to be used with this highest value of E by Stephenson (1984), and these were the data that were revisited by Smith (1991).

Two different values of ν, which is a measure of how much a material which is being stretched in one dimension contracts in the other two dimensions, were used. The usual value of ν given for ice and used by Stephenson (1984), Smith (1991) and Vaughan (1995) is 0.3. However, Jenkins and others (2006) found a value of ν close to 0.5 fitted their measured horizontal and vertical strains downstream of the grounding line of nearby Rutford Ice Stream, and which, interestingly, is the theoretical maximum, and as such assumes that the ice shelf is incompressible.

Values of $A_0(t)$ came from the results of the t_tide model, discussed below, and were taken as half the typical maximum tidal amplitude at both spring and neap tides for the study period: 2.35 and 0.62 m, respectively. The model was run for two different ice thicknesses, both taken from BEDMAP (Lythe and others, 2001): 1017 m, at the location where the CATS02.01 model was run, and 1913 m, the largest value of ice thickness at the grounding zone as mapped from interferometry (Fig. 3). The elastic beam and tidal models were run in Matlab™, and the hinge zone width calculated to the nearest 100 m.

Table 2. Principal tidal coefficients

Component		Hours	Coefficient ratio ($M_2 = 100$)
Semi-diurnal			
Principal lunar	M_2	12.42	100
Principal solar	S_2	12.00	46.6
Larger lunar elliptic	N_2	12.66	19.2
Lunisolar	K_2	11.97	12.7
Diurnal			
Lunisolar	K_1	23.93	58.4
Principal lunar	O_1	25.82	41.5
Principal solar	P_1	24.07	19.4
Elliptical lunar	Q_1	26.87	7.9
Longer period			
Lunar fortnightly	M_f	327.86	17.2
Lunar monthly	M_m	661.30	9.1

Table 3. Tidal heights at the time of acquisition of each SAR image of Evans Ice Stream

track_frame	Date	Time GMT	Tidal height cm
037_5265	23 Jan. 1994	11:26:54	–8
020_5553	25 Jan. 1994	07:13:00	–74
037_5265	26 Jan. 1994	11:36:54	–56
020_5553	28 Jan. 1994	07:13:00	13
206_5535	29 Jan. 1996	07:29:37	1
206_5535	30 Jan. 1996	07:29:38	–36
392_5553	11 Feb. 1996	07:21:15	91
392_5553	12 Feb. 1996	07:21:17	54

https://doi.org/10.3189/172756409789624292 Published online by Cambridge University Press

Table 4. The width of the grounding zone of Evans Ice Stream as modelled using an elastic beam

Ice thickness	Young's modulus	Grounding zone width	
		$v = 0.3$	$v = 0.5$
m	GPa	m	m
1017	0.88	13 200	13 900
	1.1	14 000	14 700
	9	23 700	24 900
1913	0.88	21 200	22 300
	1.1	22 500	23 600
	9	38 000	39 900

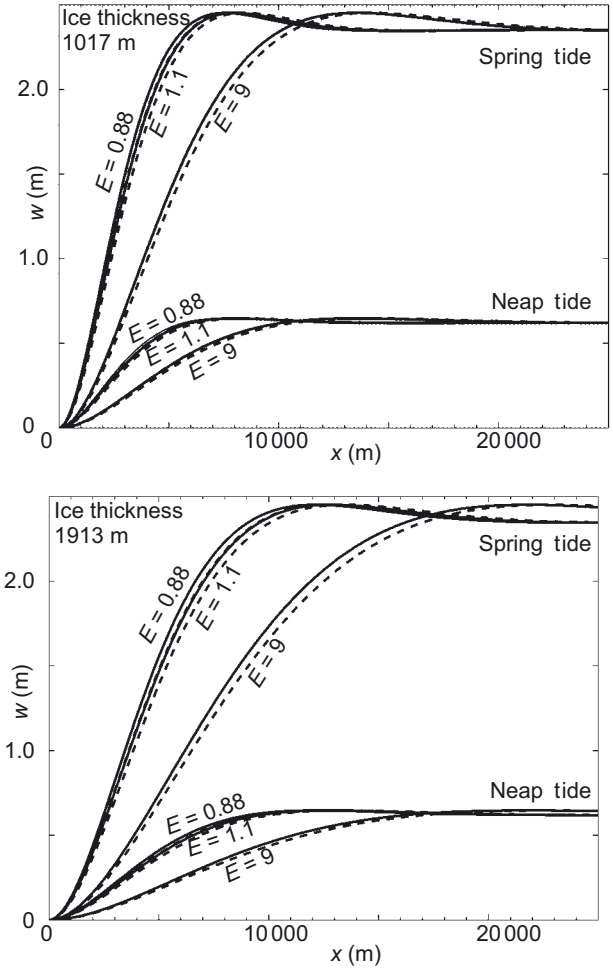

Fig. 4. Grounding zone width modelled by an elastic beam for Evans Ice Stream using ice thicknesses of 1017 and 1913 m and E of 0.88, 1.1 and 9. Solid and dashed curves indicate Poisson's ratios of 0.3 and 0.5, respectively.

RESULTS

SAR interferometry showed vertical motion in a clearly defined grounding zone (Fig. 3). The grounding zone was mapped from four SAR frames, and found to match where the frames overlapped, although the fringe rate in the grounding zone differed between flattened interferograms of different scenes, due to their different vertical tidal displacements. The grounding line has a complex shape, and runs parallel to the direction of the main trunk for ~120 km on the east side of the ice stream. The upstream end of this part of the grounding zone lies adjacent to an area of slow-moving ice, probably frozen to its bed, which divides the eastern and western groups of tributaries. A major flowline, visible in both SAR intensity images and interferograms, extends downstream from here, dividing the flow regimes from the two groups of tributaries (Fig. 3). The grounding zone to the west of this flowline is perpendicular to the direction of the main trunk and considerably wider than that on the east side. Thus, for much of the length of the main trunk, the east side of the ice stream is grounded and the west side floating.

Tidal modelling showed that the maximum tidal range for the Evans Ice Stream grounding zone is >5 m. This is well above the usual 1–2 m range for the ice shelves surrounding Antarctica, and greater than the 3 m range for the FRIS. However, Evans Ice Stream does not have as high a tidal range as the 6 m at the grounding line of nearby Rutford Ice Stream (Doake, 1992; Padman and others, 2002).

Vertical displacement observed in the interferograms was compared to the modelled tidal height differences. On the flat topography of the ice shelf, fringes due to the perpendicular baseline could be discounted because of the relatively high altitudes of ambiguity (Table 1). Although some fringes can be accounted for by LOS displacement, the changing orientation of the grounding zone and range of flow directions from the tributaries means that for most of the area the flow direction is orientated approximately perpendicular to the LOS, meaning the majority of the fringes can be explained by vertical motion. Table 1 shows vertical change in the grounding zone as calculated from the number of fringes. This is a closer match to that predicted by the tidal model for tracks 020 and 206, which are ascending frames located in similar places in 1994 and 1996, respectively, and have look directions perpendicular to the ice-stream flow direction, making them especially insensitive to horizontal displacement. In the case of the track 020 interferogram, additional fringes may have been present in the grounding zone had the scene extended further north. It is clear that the ice shelf is being affected by vertical motion proportional to changing tidal height.

The width of the grounding zone calculated using the elastic beam model was compared to the mapped values, which were measured using tools in ArcGIS both parallel to the ice-flow direction and perpendicular to both F and H (Table 4; Fig. 4). The choice of $A_0(t)$ does not affect the modelled width of the grounding zone, which is consequently the same for spring and neap tides (Fig. 4). Increasing values of E and v lead to an increase in the modelled width. Using $v = 0.5$ and $E = 0.88$ produced very similar results to using $v = 0.3$ and $E = 1.1$. The grounding zone nearest to where the tidal model was run, where the ice thickness was 1017 m, was found to best fit a model using $E = 0.88$ and $v = 0.3$. This was the case for most of the rest of the grounding zone. However, much further upstream, at the mapped grounding zone where the maximum ice thickness was 1913 m, the mapped width best fits a model with $E = 1.1$ and v between 0.3 and 0.5. Using values of v for ice other than 0.3 should therefore be considered in future work. As suspected, using $E = 9$ vastly overestimates the width of the grounding zone and thus laboratory-derived values of E for ice are unsuitable for use in this type of work.

https://doi.org/10.3189/172756409789624292 Published online by Cambridge University Press

DISCUSSION

Inconsistencies between previously published versions of the Evans grounding line were noted prior to this study. Grounding lines by Vaughan and others (2003) and Joughin and others (2006) overlap with the grounding zone derived here, although they differ by up to 9 km, but the grounding line derived from the MODIS (moderate-resolution imaging spectroradiometer) Mosaic of Antarctica (MOA) (T. Haran and others, http://nsidc.org/data/nsidc-0280.html) is as much as 93 km downstream of these and clearly on the floating ice shelf (Fig. 2).

Vaughan's grounding line, and probably also Joughin's, were digitized from interferograms, although whether they defined F or H is unknown, and the MOA grounding line was identified from the break in slope between grounded and floating ice (personal communication from NSIDC, 2007). It is not the case that the three grounding lines differ due to picking out different combinations of F, G, I and H, as interferometry maps the zone between F and H, so methods locating either G or I would locate their grounding lines within the hinge zone as mapped from interferometry. It is more useful to map the grounding zone, rather than a line, as this provides additional information by showing its shape and width.

Several widely used datasets of Antarctica also position the grounding line of Evans Ice Stream considerably further downstream than observed in SAR interferometry of 1994 and 1996. The Vaughan and others (2003) and Joughin and others (2006) grounding lines, although close to the grounding zone derived in this study, are not part of widely used datasets. The BEDMAP dataset (Lythe and others, 2001), for example, defines the grounding line as far as 37 km further downstream than even the MOA grounding line, or up to 100 km from the grounding zone as mapped in this study, as shown by the seaward limit of the grounded bed layer and the landward limit of the water depth layer. This imprecision clearly affects any work using the BEDMAP dataset as an input. Similarly, the landward limit of the bathymetry grid in the CATS02.01 model, which is in a similar place to the grounding line of Lythe and others (2001), meant that tidal components used in this study were extracted from the CATS02.01 model at a latitude of –76.75° and a longitude of –76.00° (Fig. 2), rather than for a coordinate closer to the mapped grounding zone. Whether the ice thickness used for the elastic beam model came from this location or from the mapped grounding zone made a difference of up to 9 km in the modelled width of the hinge zone, for realistic values of E.

Although ice thickness and basal topography are known to affect grounding zone width (Fricker and Padman, 2006), in the case of Evans Ice Stream this may also apply to its shape. On the eastern side of the main trunk, where the hinge zone is further downstream, the bed is shallower than on the western side, with depths of, for example, 1249 m compared to 1546 m. The ice-surface elevation is only slightly higher on the eastern side, for example, 235 m compared to 201 m, and as such ice on the western side is thicker, for example, 1787 m compared to 1475 m (Lythe and others, 2001), leading to a wider grounding zone.

As well as the shape of the grounding zone, tidal conditions are also an important regulator of ice-stream flow. Gudmundsson (2007) expected Evans Ice Stream to show fortnightly tidal variations in velocity similar to those of nearby Rutford Ice Stream, and as the tidal range at the Evans grounding line is almost as high, this is clearly worthy of further investigation.

SUMMARY

Evans Ice Stream has a grounding zone with a complex shape, which may be governed by its bed topography and the flow of its five tributaries. SAR interferometry maps the grounding zone up to 100 km upstream of its location in some widely used datasets, and the grounding zone is 6–23 km wide. Evans Ice Stream has a significant tidal range, 5 m, and vertical motion of the ice stream due to tidal forcing is clearly taking place. Finally, it is clear that remote-sensing and modelling methods allow much to be learnt about ice streams where adverse conditions hamper extensive field campaigns, although further work is required to resolve discrepancies between datasets.

ACKNOWLEDGEMENTS

Thanks to G. Aðalgeirsdóttir, M. King and K. Makinson for valuable advice on the tidal model. SAR data were obtained through the VECTRA project. Helpful and constructive comments from C. Clark and from two anonymous reviewers are much appreciated.

REFERENCES

Anandakrishnan, S., D.E. Voigt, R.B. Alley and M.A. King. 2003. Ice Stream D flow speed is strongly modulated by the tide beneath the Ross Ice Shelf. *Geophys. Res. Lett.*, **30**(7), 1361. (10.1029/2002GL016329.)

Bamber, J.L., D.G. Vaughan and I. Joughin. 2000. Widespread complex flow in the interior of the Antarctic ice sheet. *Science*, **287**(5456), 1248–1250.

Bindschadler, R. 2006. The environment and evolution of the West Antarctic ice sheet: setting the stage. *Philos. Trans. R. Soc. London, Ser. A*, **364**(1844), 1583–1605.

Bindschadler, R.A., M.A. King, R.B. Alley, S. Anandakrishnan and L. Padman. 2003. Tidally controlled stick–slip discharge of a West Antarctic ice stream. *Science*, **301**(5636), 1087–1089.

Doake, C.S.M. 1992. Gravimetric tidal measurement on Filchner Ronne Ice Shelf. *FRISP Rep.*, 34–39.

Fricker, H.A. and L. Padman. 2006. Ice shelf grounding zone structure from ICESat laser altimetry. *Geophys. Res. Lett.*, **33**(15), L15502. (10.1029/2006GL026907.)

Gudmundsson, G.H. 2006. Fortnightly variations in the flow velocity of Rutford Ice Stream, West Antarctica. *Nature*, **444**(7122), 1063–1064.

Gudmundsson, G.H. 2007. Tides and the flow of Rutford Ice Stream, West Antarctica. *J. Geophys. Res.*, **112**(F4), F04007. (10.1029/2006JF000731.)

Jenkins, A., H.F.J. Corr, K.W. Nicholls, C.L. Stewart and C.S.M. Doake. 2006. Interactions between ice and ocean observed with phase-sensitive radar near an Antarctic ice-shelf grounding line. *J. Glaciol.*, **52**(178), 325–346.

Joughin, I. and J.L. Bamber. 2005. Thickening of the ice stream catchments feeding the Filchner–Ronne Ice Shelf, Antarctica. *Geophys. Res. Lett.*, **32**(17), L17503. (10.1029/2005GL023844.)

Joughin, I., J.L. Bamber, T. Scambos, S. Tulaczyk, M. Fahnestock and D.R. MacAyeal. 2006. Integrating satellite observations with modelling: basal shear stress of the Filcher–Ronne ice streams, Antarctica. *Philos. Trans. R. Soc. London, Ser. A*, **364**(1844), 1795–1814.

Lythe, M.B., D.G. Vaughan and BEDMAP consortium. 2001. BEDMAP: a new ice thickness and subglacial topographic model of Antarctica. *J. Geophys. Res.*, **106**(B6), 11,335–11,351.

Padman, L., H.A. Fricker, R. Coleman, S. Howard and L. Erofeeva. 2002. A new tide model for the Antarctic ice shelves and seas. *Ann. Glaciol.*, **34**, 247–254.

https://doi.org/10.3189/172756409789624292 Published online by Cambridge University Press

Pawlowicz, R., B. Beardsley and S. Lentz. 2002. Classical tidal harmonic analysis including error estimates in MATLAB using T_TIDE. *Comput. Geosci.*, **28**(8), 929–937.

Reeh, N., E. Lintz Christensen, C. Mayer and O.B. Olesen. 2003. Tidal bending of glaciers: a linear viscoelastic approach. *Ann. Glaciol.*, **37**, 83–89.

Rignot, E. 1998. Radar interferometry detection of hinge-line migration on Rutford Ice Stream and Carlson Inlet, Antarctica. *Ann. Glaciol.*, **27**, 25–32.

Schoof, C. 2007. Ice sheet grounding line dynamics: steady states, stability, and hysteresis. *J. Geophys. Res.*, **112**(F3), F03S28. (10.1029/2006JF000664.)

Smith, A.M. 1991. The use of tiltmeters to study the dynamics of Antarctic ice-shelf grounding lines. *J. Glaciol.*, **37**(125), 51–58.

Stephenson, S.N. 1984. Glacier flexure and the position of grounding lines: measurements by tiltmeter on Rutford Ice Stream, Antarctica. *Ann. Glaciol.*, **5**, 165–169.

Vaughan, D.G. 1994. Investigating tidal flexure on an ice shelf using kinematic GPS. *Ann. Glaciol.*, **20**, 372–376.

Vaughan, D.G. 1995. Tidal flexure at ice shelf margins. *J. Geophys. Res.*, **100**(B4), 6213–6224.

Vaughan, D.G., A.M. Smith, P.C. Nath and E. Le Meur. 2003. Acoustic impedance and basal shear stress beneath four Antarctic ice streams. *Ann. Glaciol.*, **36**, 225–232.

Vieli, A. and A.J. Payne. 2005. Assessing the ability of numerical ice sheet models to simulate grounding line migration. *J. Geophys. Res.*, **110**(F1), F01003. (10.1029/2004JF000202.)

Weertman, J. 1974. Stability of the junction of an ice sheet and an ice shelf. *J. Glaciol.*, **13**(67), 3–11.

Zebker, H.A., P.A. Rosen, R.M. Goldstein, A. Gabriel and C.L. Werner. 1994. On the derivation of coseismic displacement fields using differential radar interferometry: the Landers earthquake. *J. Geophys. Res.*, **99**(B10), 19,617–19,634.

https://doi.org/10.3189/172756409789624292 Published online by Cambridge University Press